Radiation-induced formation of DNA intrastrand crosslinks between thymine and adenine bases: a theoretical approach

Bertrand Xerri,[a] Christophe Morell,[a] André Grand,[a] Jean Cadet,[a] Paola Cimino†[b] and Vincenzo Barone*[b]

Received 28th June 2006, Accepted 7th September 2006
First published as an Advance Article on the web 29th September 2006
DOI: 10.1039/b609134b

The role of local geometric and stereo-electronic effects in tuning the radiation-induced formation of intrastrand crosslinks between adenine and thymine has been analyzed by a computational approach rooted in density functional theory. Our study points out that together with steric accessibility, stereo-electronic effects play a major role in determining the reaction mechanism and the observed predominance of the thymine–adenine lesion over the opposite sequence isomer.

1. Introduction

Tandem modifications represent a subclass of complex DNA clustered lesions that have been shown to be mostly generated by exposure of cells to high energy radiation ($E > 100$ keV) including X- and γ-rays together with high linear transfer energy (LET) particles.[1–3] Formation of the latter damage is mostly explained by multiple events associated with the deposit of energy along the particle track. However, evidence has been provided in particular through the pioneering work of Box and co-workers that one ·OH radical hit is able to generate tandem base lesions in short oligonucleotides and isolated DNA.[4] Formylamine (Fo), a pyrimidine remnant of ·OH and one-electron oxidation-mediated decomposition reactions of thymine and cytosine[5,6] has been shown to be part of tandem base lesions together with 8-oxo-7,8-dihydroguanine (8-oxoguanine) within short oligonucleotides and DNA exposed to ionizing radiation and type I photosensitizers in aerated aqueous solutions.[7–9] It was shown that both 5-hydroxy and 6-hydroxy-6(5)-peroxy-5,6-dihydropyrimidyl radicals are involved in the intramolecular addition to the C8 position of the vicinal guanine moiety giving rise, through secondary reactions, to the Fo/8-oxoguanine and 8-oxoguanine/Fo tandem lesions.[8] Insights into the mutagenic features of the latter tandem damage and the specificity of enzymic removal by base excision repair proteins were gained from studies that have required the site-specific insertion of these lesions in defined-sequence oligonucleotides.[10,11] Other vicinal base modifications have been shown to be generated under oxidative conditions. This involves in particular the formation of a cross-link lesion between the 5′ cytosine and the N4 nitrogen of the 3′ cytosine in 2′-deoxycytidylyl (3′–5′) 2′-deoxycytidine (dCpdC) upon type I photosensitization.[12] Another tandem lesion between two adjacent cytosines in one-electron photo-oxidized dCpdC has been isolated and characterized.[13] This was accounted for by the covalent attachment of the N3-centred radical of the 3′ cytosine to the C6 atom of the 5′ cytosine. Considerable attention has been devoted to the formation and biochemical features of tandem lesions whose generation involves intramolecular cyclization of a 2-deoxyribose radical that arises from radical hydrogen abstraction within the 5′-hydroxymethyl group of a nucleoside to either the C8 carbon of purine bases or the C6 of pyrimidine bases. Thus, it was found that both (5*R*) and (5*S*) diastereomers of 5′,8-cyclo-2′-deoxyadenosine and 5′,8-cyclo-2′-deoxyguanosine are generated in oxygen-free aqueous solutions.[14–18] In addition, several diastereomers of 5′,6-cyclo-5,6-dihydropyrimidine nucleosides were shown to be produced by γ radiation of thymidine and 2′-deoxycytidine in frozen aqueous solutions at 196 K[19] and further inserted into defined sequence oligonucleotides.[20,21] Interestingly, two diastereomers of 5′,6-cyclo-5′-hydroxy-5,6-dihydro-2′-deoxyuridine were isolated and characterized in γ-irradiated aerated aqueous solutions of 2′-deoxycytidine.[22] More recently the two latter pyrimidine cyclonucleosides were site-specifically incorporated into defined sequence DNA fragments.[23] It may be added that other tandem base lesions whose mechanism of formation is rationalized in term of addition of 5-(uracilyl)methyl radical[6] to vicinal purine bases have been recently characterized in dinucleoside monophosphates and isolated DNA.[24–26] Subsequently, it was also shown that the related radical that may derive from the predominant deprotonation of the methyl group of the pyrimidine radical cation of 5-methyl-2′-deoxycytidine[27] is able to add to the vicinal guanine base giving rise to tandem base modifications in dinucleoside monophosphates and DNA fragments.[28,29]

In spite of the studies mentioned above, there is still a lack of mechanistic insight into the radical formation of the latter classes of intra-strand tandem lesions that involve the covalent attachment of thymine or 5-methylcytosine to a vicinal purine base. Therefore the present study is aimed at gaining information on the reaction pathways involved in the radiation-induced formation of two isomeric thymine–adenine cross-links, namely TÂ and AT̂ adducts[24,25] that arise from the attachment of the 5-(uracilyl)methyl radical to the C8 of the purine base. This was achieved using a theoretical approach.

Thanks to the recent advances of quantum mechanical methods rooted in density functional theory (DFT),[30,31] systems of biological and pharmacological interest can be nowadays treated within remarkable accuracy, a particularly effective approach being

[a]*Laboratoire Lésions des Acides Nucléiques, SCIB-UMR no. 3 (CEA/UJF) Département de Recherche Fondamentale sur la Matière Condensée, CEA/Grenoble, 17 Avenue des Martyrs, 38054, Grenoble cedex 9, France*
[b]*Dipartimento di Chimica, Università di Napoli Federico II, Complesso Universitario Monte S. Angelo, Via Cintia, 80128, Napoli, Italy. E-mail: baronev@unina.it*
† Permanent address: Dipartimento di Scienze Farmaceutiche, Università di Salerno, Via Ponte don Melillo, 84084, Fisciano (SA), Italy

offered by hybrid functionals (here B3LYP) with medium size basis sets [here 6–31G(d,p)]. In that respect, it may be pointed out that a similar theoretical approach, based on the use of the DFT (B3LYP) formalism, was applied to investigate the mechanism of radiation formation of other tandem lesions including purine 5′,8-cyclonucleosides and pyrimidine 5′,6-cyclonucleosides.[32] Thus, we have performed a comprehensive study of the reaction mechanism leading to tandem lesions of suitable models of adenine–thymine (A–T) and thymine–adenine (T–A) pairs using this computational model. Despite the quite large dimensions of the model used to mimic the reaction center (*vide infra*) more distant parts of DNA chains can influence the reaction by steric and/or electrostatic interactions. We are, however, convinced that local stereo-electronic effects play a significant role in tuning this kind of reaction and that their analysis represents a mandatory starting point for successive analysis of long range effects by suitable QM/MM and/or continuum models.

2. Methods

Computational details

All the calculations were carried out using the Gaussian 03 package[33] at B3LYP/6–31G(d,p)[34] level. After full geometry optimization, the different stationary points were characterized as minima or transition states by calculating the harmonic vibrational frequencies. Zero point energies (ZPEs) and thermal contributions to thermodynamic functions and activation parameters were computed from those structures and harmonic frequencies by using the rigid rotor/harmonic oscillator approximation and the standard expressions for an ideal gas in the canonical ensemble at 298.15 K and 1 atm. Reaction paths were characterized at the same level in terms of the intrinsic reaction coordinate (IRC)[35] starting from the optimized transition structure (TS) and using 10 steps in each direction, with a step size of 0.3 $amu^{-1/2}$ Bohr.

3. Results and discussion

As mentioned above, there is convincing experimental evidence showing that the reaction under investigation begins with the homolytic cleavage of the C–H bond in the thymine methyl group with the consequent formation of a radical (R). Then, the characterized final product presents an intermolecular bond between the thymine–CH_2 radical and the C8 atom of the adjacent adenine, but different sequences of the DNA bases adenine (A) and thymine (T) in the nucleic acidic strand lead to different percentages of final product: 85% with 5′-AT-3′ and 15% with 5′-TA-3′.

In the absence of experimental data concerning the structures of reaction intermediates and transition states, a rationalization of these results in terms of reaction mechanisms can be obtained, in our opinion, by a comparative theoretical analysis of different paths taking into account the available experimental evidences. As a first step, we have carefully selected a suitable model including all the local interactions which can play a role in tuning the reaction mechanism. After some tests, we ended up with the two dinucleoside monophosphates (5′-AT-3′ and 5′-TA-3′) shown in Scheme 1: they include the two nucleic bases [adenine (A) and thymine (T)] each covalently attached to a sugar residue namely the 2-deoxyribose, together with the phosphodiester bridge connecting the two residues.

As mentioned above, elimination of a hydrogen atom from the methyl group of adenine leads to the radical species (R–AT and R–TA) which are the starting points of our mechanistic investigation.

Full geometry optimization of the R–AT and R–TA systems leads to a distance between the bases much longer than the experimental values due to the lack of the constraints introduced

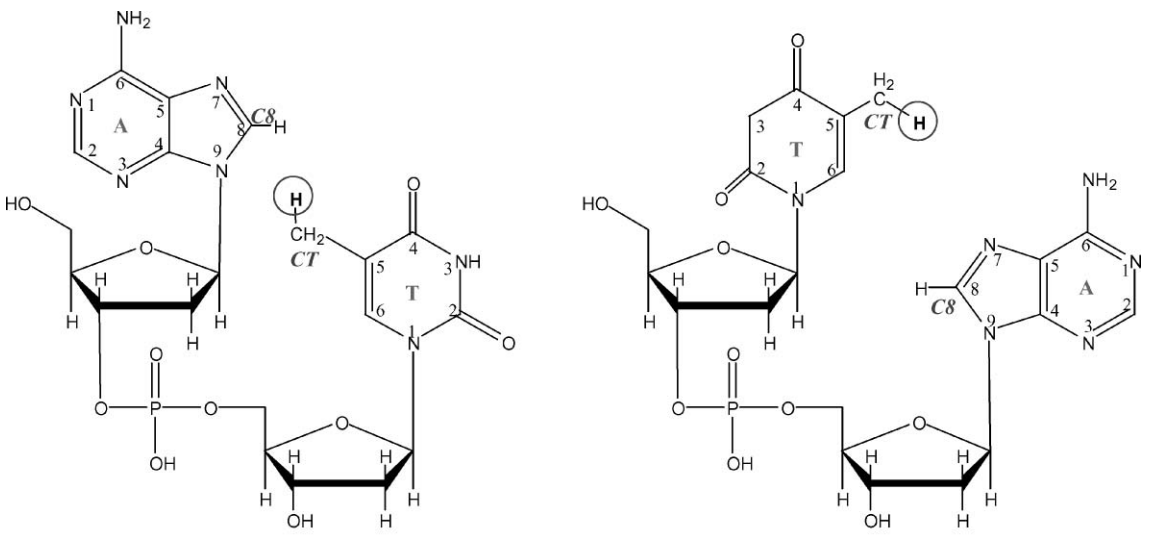

Scheme 1 Structures of the studied dinucleoside monophosphates 5′-AT-3′ and 5′-TA-3′. Elimination of the circled H atoms leads to the R–AT and R–TA species.

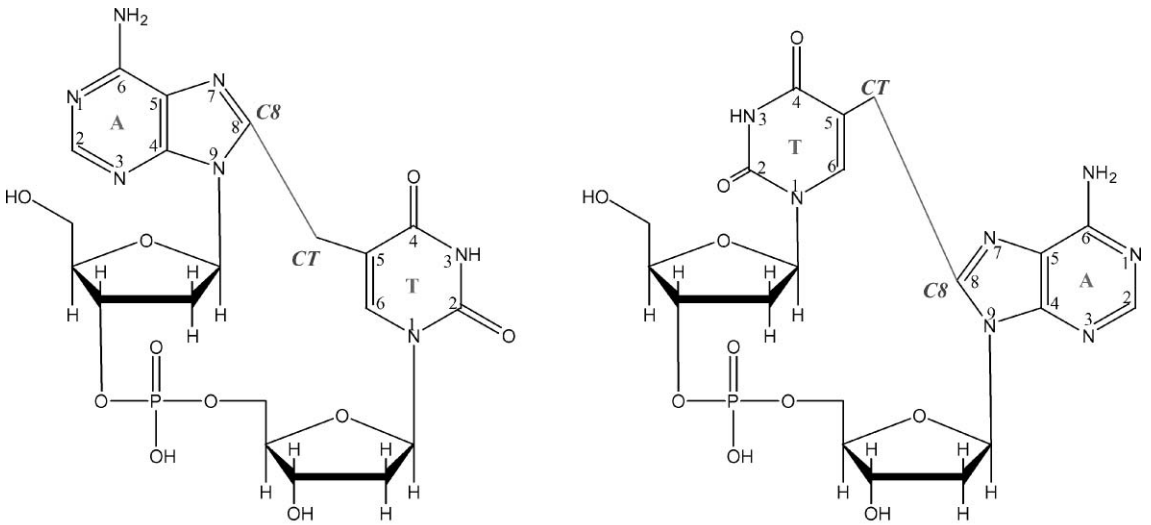

Scheme 2 Structures of the studied dinucleoside monophosphate products of AT̂ and TÂ tandem lesions.

by the DNA sequence. As a consequence the energies of these systems should be considered with some caution in the following evaluation of thermodynamic and kinetic parameters. However, the computed stabilities of R–AT and R–TA are so close to suggest that specific interactions are negligible and that our model is sufficient to obtain a realistic reaction mechanism.

In the next two subsections the mechanisms of the AT̂ and TÂ tandem lesions (the final products are shown in Scheme 2) will be considered separately, whereas the last subsection is devoted to a comparison between the two situations.

3.1 AT̂ tandem lesion

As already discussed, the first step consists in the formation of the R–AT radical; so, starting from this species the general scheme for the reaction is the following:

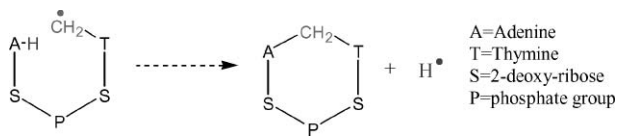

On the basis of our computations, the stepwise pathway for the reaction can be described in terms of an addition–elimination mechanism, characterized by two successive steps, *i.e.* the formation of the bond between the C8 atom of adenine and the methyl carbon of thymine (CT) followed by the breaking of the bond between C8 and its hydrogen atom H8.

The transition state (TS1–AT, Fig. 1) governing the first step (essentially formation of a CT–C8 bond) is characterized by an incipient tetrahedral character of C8 (sp2 hybridization in adenine and sp3 hybridization in the first intermediate), a lengthening of the N7–C8 bond (to 1.377 Å) which is evolving from a double to a single bond, and a distance of 2.142 Å between CT and C8.

Table 1 Thermodynamic and kinetic parameters for the formation of the AT̂ tandem lesion at standard conditions (298.15 K, 1 atm) in the gas phase computed at the B3LYP/6–31G(d,p) level

	TS1–R	I1–R	TS2–I1	P–I1	P–R
ΔE/kcal mol^{-1}	41.5	8.6	37.2	34.8	43.3
$T\Delta S$/kcal mol^{-1}	−3.8	−2.5	0.95	7.9	5.4
ΔG/kcal mol^{-1}	44.2	10.6	36.7	28.2	38.7

This step ends with the formation of a relatively stable intermediate (I1–AT, Fig. 1) in which the C8–CT and C8–H8 bond lengths are 1.560 and 1.093 Å, respectively. Starting from this intermediate, the reaction proceeds toward a second transition state (TS2–AT, Fig. 1) issuing from the breaking of the C8–H8 bond of adenine characterized by a distance of 1.916 Å (C8–CT is 1.506 Å).

After that, the reaction leads to the AT̂ tandem lesion observed experimentally (P–AT, Fig. 1).

The energetic of all the reaction steps is sketched in Fig. 2 and Table 1.

The energy barrier ($\Delta E^{\ddagger}_{(TS1-R)}$) governing the first step is of 41.5 kcal mol^{-1} (Fig. 2) and the corresponding free energy of activation ($\Delta G^{\ddagger}_{(TS1-R)}$) amounts to 44.2 kcal mol^{-1} (Table 1) with a quite small negative entropy contribution ($T\Delta S^{\ddagger}_{(TS1-R)} = -3.8$ kcal mol^{-1}) probably related to the decreased flexibility of the whole structure. This step ($\Delta E_{(I1-R)}$) is endoergic by 8.6 kcal mol^{-1} and is further disfavored by a small entropy contribution ($T\Delta S_{(I1-R)} = -2.5$ kcal mol^{-1}) leading to $\Delta G_{(I1-R)} = 10.6$ kcal mol^{-1}. All these quantities are quite close to those obtained by Durbeej and Eriksson for similar systems.[36,37]

The second reaction step (Fig. 2, Table 1) is characterized by an activation free energy ($\Delta G^{\ddagger}_{(TS2-I1)}$) of 36.7 kcal mol^{-1} ($\Delta G^{\ddagger}_{(TS2-R)} = 47.3$ kcal mol^{-1} with respect to reactants) and is now favored by entropic effects ($T\Delta S^{\ddagger}_{(TS2-R)} = 0.95$ kcal mol^{-1}) due to some reduction of the overall rigidity. The corresponding reaction free

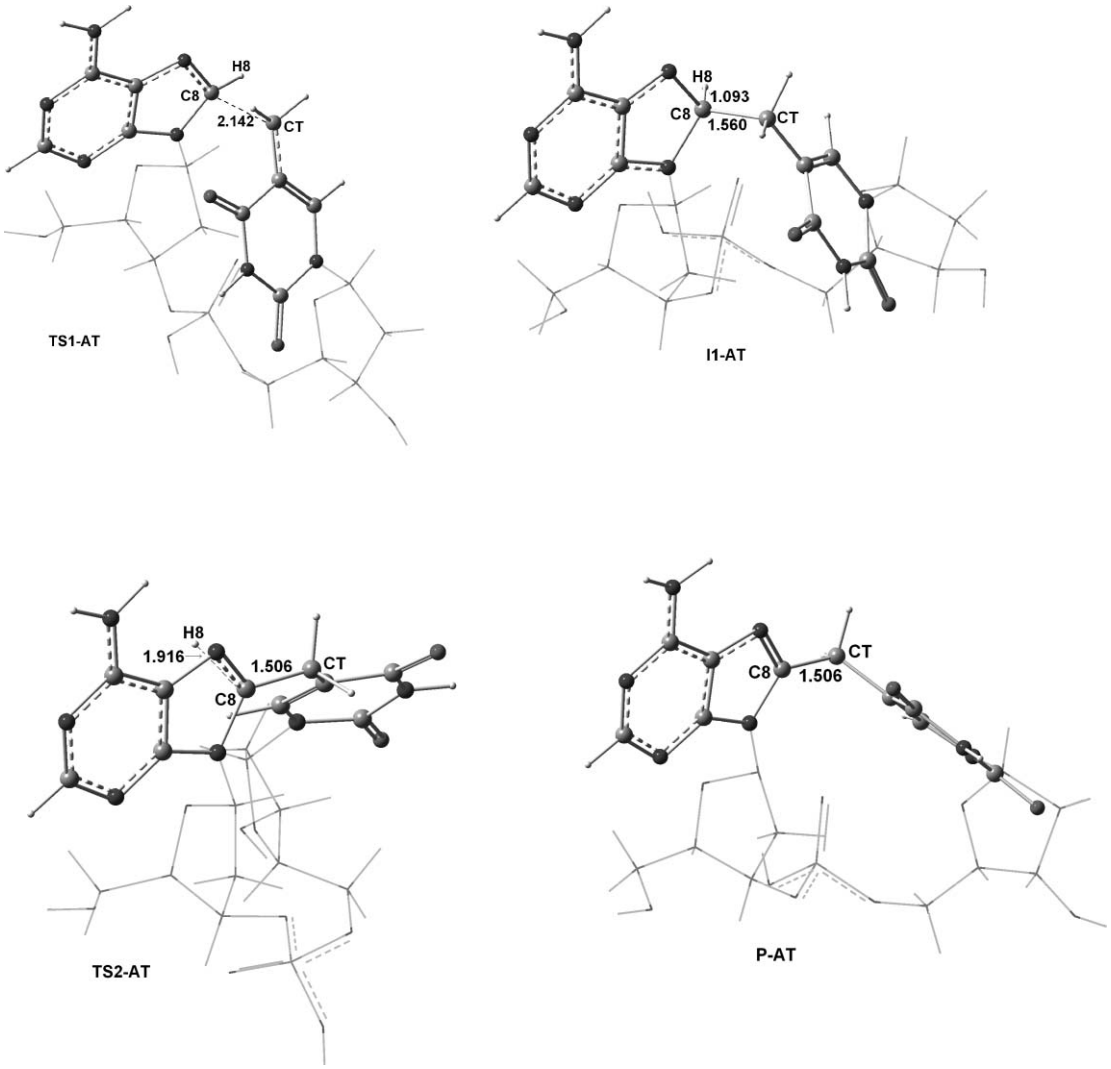

Fig. 1 Optimized structures of: transition state TS1-AT, intermediate I1-AT, transition state TS2-AT and product P–AT (the distances are in Å).

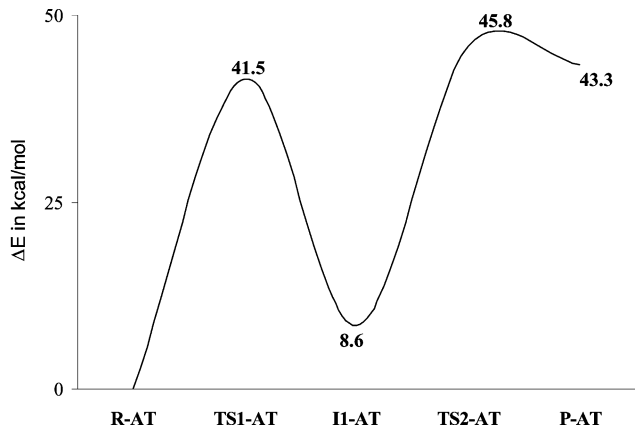

Fig. 2 Computed electronic energies (ΔE and $\Delta E^{\ddagger}$) of reaction steps characterizing in the mechanism of the AT̂ tandem lesion at the B3LYP/6–31G(d,p) level.

energy ($\Delta G_{(P-I2)}$) is 28.2 kcal mol^{-1} ($\Delta G_{(P-R)}$ = 38.7 kcal mol^{-1} with respect to reactants): thus the overall reaction is strongly endothermic.

3.2 TÂ tandem lesion

The second title reaction can be formally written as:

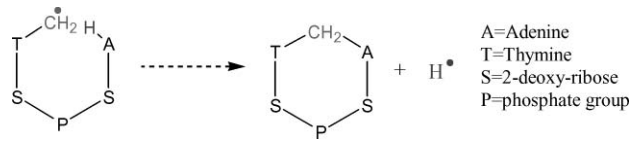

Our computations show that this reaction channel is more involved than the previous one since, after a quite similar first reaction step, the H8 atom does not leave from the substrate (C8–H8 = 1.098 Å), but is, rather, transferred on the thymine leading to a second intermediate, which, in turn, can evolve along different routes. In detail, starting from the R–TA radical (Scheme 1), the transition state TS1–TA (C8–CT = 2.158 Å, Fig. 3) rules the formation of the covalent inter-base bond (C8–CT = 1.561 Å) in the intermediate I1–TA (Fig. 3).

Next, the second step involves the cleavage of the C8–H8 bond, and, through the transition state TS2–TA (C8–H8 = 1.990 Å, Fig. 3), leads to a second intermediate (I2–TA, Fig. 3) in which H8 is bonded to the C5 of thymine (C5–H8 = 1.097 Å) in agreement

Table 2 Thermodynamic and kinetic parameters for the formation of the TÂ tandem lesion at standard conditions (298.15 K, 1 atm) in gas-phase computed at the B3LYP/6–31G(d,p) level

	TS1–R	I1–R	TS2–I1	I2–R	TS3a–I2	TS3b–I2	Pa–I2	Pb–I2
ΔE/kcal mol^{-1}	39.3	12.1	36.0	11.0	21.4	15.6	18.5	−9.9
$T\Delta S$/kcal mol^{-1}	−2.83	−0.06	−1.47	−4.49	3.24	1.36	10.45	3.5
ΔG/kcal mol^{-1}	41.6	12.6	37.2	13.4	20.0	15.4	11.2	−12.6

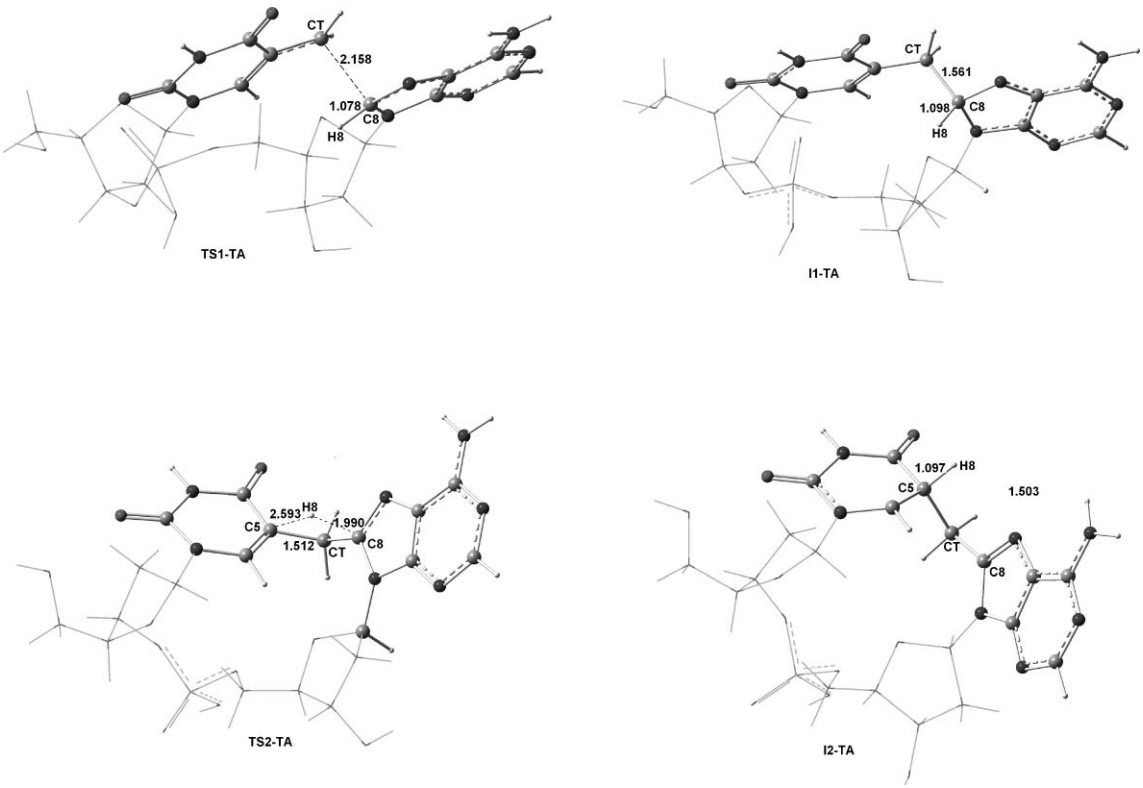

Fig. 3 Optimized structures of: transition state TS1–TA, intermediate I1–TA, transition state TS2–TA and intermediate I2–TA (the distances are in Å).

with previous computational studies and experimental evidences.[38] As a matter of fact, in TS2–TA the distance of H8 from the C5 atom thymine is 2.593 Å.

Starting from I2–TA, two reaction channels are open. The first one corresponds to the homolytic cleavage of the C5–H8 bond, which, through the transition state TS3a–TA (characterized by a C5–H8 distance of 1.992 Å, Fig. 4), leads to the formation of the TÂ tandem lesion (Pa–TA, Fig. 4).

The second channel involves, instead, the breaking of the C5–CT bond through the transition state TS3b–TA (characterized by a C5–CT bond length of 2.139 Å, Fig. 4) and the formation of a dinucleoside involving uracil (U) and a 8-methylated adenine residue with a radical site at position 8 (Pb–TA, Fig. 4).

Of course, the radical form of methylated adenine will spontaneously react for instance for generating the neutral methylated adenine through reaction with the hydrogen atoms largely available in the reaction medium. The energetic of all the reaction steps is sketched in Fig. 5 and Table 2.

The first step (Fig. 5, Table 2) involves an activation energy, $\Delta E^{\ddagger}_{(TS1-R)}$, of 39.3 kcal mol^{-1} ($\Delta G^{\ddagger}_{(TS1-R)} = 41.6$ kcal mol^{-1}; Table 2) and a reaction energy, $\Delta E_{(I1-R)}$, of 12.1 kcal mol^{-1} ($\Delta G_{(I1-R)} = 12.6$ kcal mol^{-1}). Once again, the entropic contribution is negligible from a thermodynamic point of view, but slows down the kinetics of the reaction due to an increased rigidity of the transition state with respect to the reactant. The second step (Fig. 5 and Table 2), involving the splitting of the C8–H bond and the formation of the C5–H bond, is characterized by $\Delta E^{\ddagger}_{(TS2-I1)} = 36.0$ kcal mol^{-1} and a reaction energy ($\Delta E_{(I2-R)}$) of 11.0 kcal mol^{-1}. Now, however, entropic terms modify also the thermodynamics of the reaction ($\Delta G_{(I2-R)} = 13.4$ kcal mol^{-1}) since the intermediate I2–TA is significantly more rigid than its I1–TA counterpart.

At this point the reaction can follow two alternative routes (Fig. 5 and Table 2). The first one leads to the TÂ tandem lesion through the cleavage of the C5–H bond with $\Delta E^{\ddagger}_{(TS3a-I2)} = 21.4$ kcal mol^{-1} and $\Delta G^{\ddagger}_{(TS3a-I2)} = 20$ kcal mol^{-1}. The reaction energy $\Delta E_{(Pa-I2)}$ is 18.5 kcal mol^{-1} ($\Delta G_{(Pa-I2)} = 11.2$ kcal mol^{-1}), but the entropic contribution $T\Delta S_{(Pa-I2)}$ (10.4 kcal mol^{-1}) is significant since a monomolecular system is transformed into a bimolecular one. The second route, leading to the cleavage of the C5–CT bond, is characterized by $\Delta E^{\ddagger}_{(TS3b-I2)}$ and $\Delta E_{(TS3b-I2)}$ of 15.6 kcal mol^{-1} and −9.9 kcal mol^{-1}, respectively. Since this step is monomolecular, the entropic contribution is much smaller ($T\Delta S_{(TS3b-I2)} = 3.5$ kcal mol^{-1}) than in the previous case (10.4 kcal mol^{-1}). Thus, formation of uracil and methylated adenine is favored with respect to TÂ

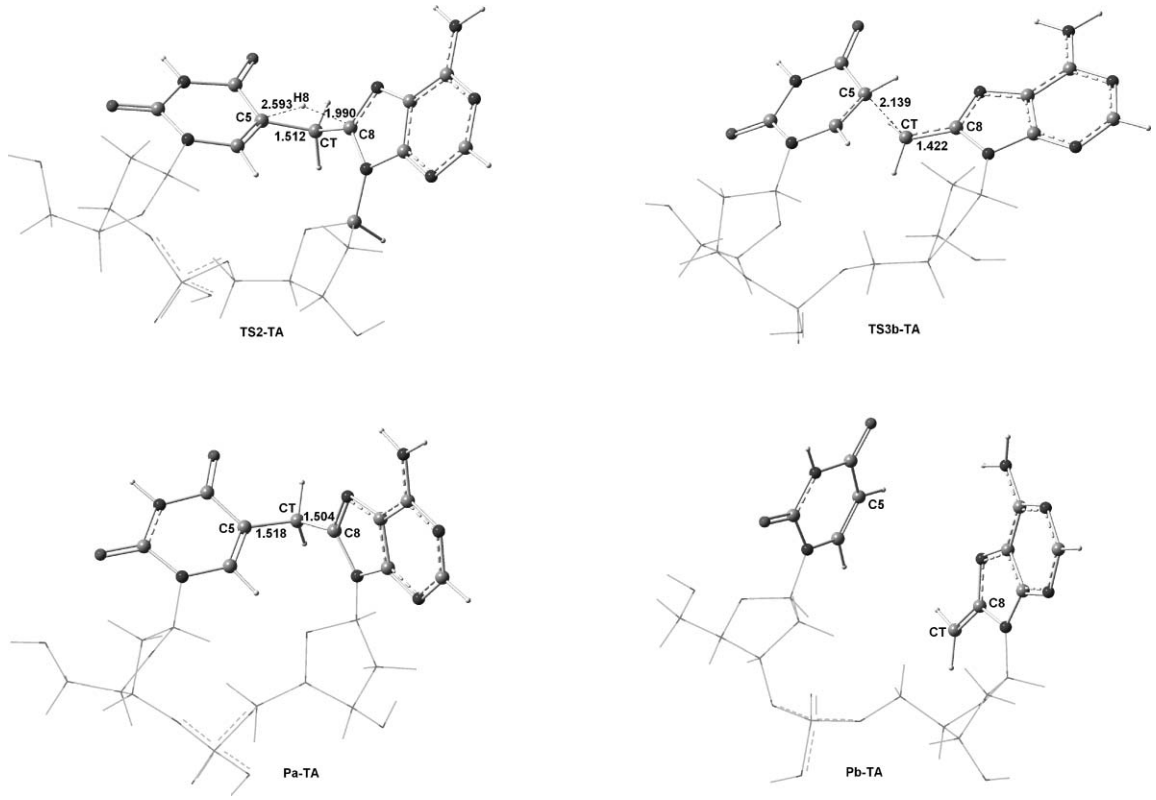

Fig. 4 Optimized structure of the transition states TS3a-TA and TSA3b–TA, and products Pa–TA and Pb–TA (the distances are in Å).

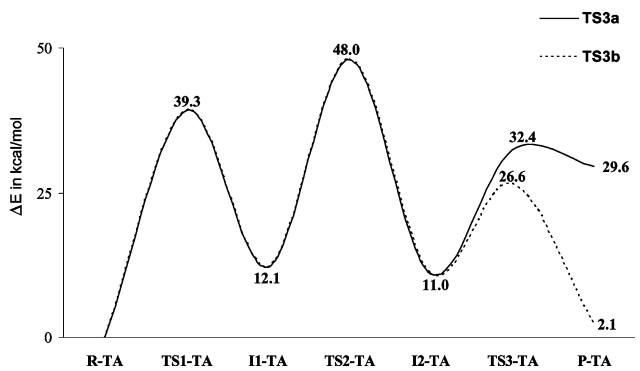

Fig. 5 Computed electronic energies (ΔE and $\Delta E^{\ddagger}$) of the reaction steps characterizing the mechanism of the TÂ tandem lesion at the B3LYP/6–31G(d,p) level.

tandem lesion by both kinetic and thermodynamic points of view.

3.3 Discussion

The results of the preceding sections show that the formation of AT̂ and TÂ tandem lesions is determined by two factors:

A geometric factor related to the DNA sequence;

A stereo-electronic factor related to the different reactivity of the dinucleoside monophosphates

The 'sequence factor' leads to two different intermediates (Fig. 1 and 3) characterized by similar structures, but showing a specific difference, which plays a dominant role in the second step of the reaction. As a matter of fact, only in the 5′-AT-3′ sequence the reactive hydrogen H8 occupies a position external to the molecular surface of the nucleoside and thus quite favorable for an attack by other radical species present in the reaction medium. On the other hand, in the 5′-TA-3′ sequence the hydrogen atom is well within the molecular envelope and thus transfer to C5 is favored with respect to extraction by external radicals.

Next, our computations show that the selection between TÂ and AT̂ tandem lesions occurs during the second reaction step, since the first one (formation of the C8–CT covalent bond) is very similar for the alternative routes concerning both structural and energetic aspects. In particular, formation of methylated adenine seems favored when starting from the R–TA reactant whereas this channel is not available starting from R–AT. This would explain why mostly AT̂ tandem lesions are experimentally observed. However, full validation of the suggested mechanism would require the experimental observation of uracil among the reaction products.

A last point deserving some comment is the role played by long range intra-molecular interactions and by solvent effects in tuning the reaction mechanism. While a proper account of steric interactions would require explicit inclusion of larger DNA models by, *e.g.* QM/MM methods, a rough evaluation of the role played electrostatic effects can be obtained employing a polarizable continuum description of the environment.[39–41] As a matter of fact, the dipole moments of transition states and intermediates collected in Table 3 indicate that some structures are significantly more polar and could be, therefore, selectively stabilized by the presence of a polar environment.

Table 3 Dipole moments (in Debyes) of intermediates and transition states computed in the gas-phase at the B3LYP/6–31G(d,p) level

TS1_AT	I1_AT	TS2_AT	P_AT	TS1_TA	I1_TA	TS2_TA	I2_TA	TS3a_TA	TS3b_TA	Pa_TA	Pb_TA
7.55	3.44	2.01	3.34	5.89	5.46	2.32	2.94	2.19	2.99	2.18	3.48

We have thus performed some PCM computations for the TSs, intermediates, and products which are characterized by a full or incipient chemical bond linking the bases. The results obtained using methylene chloride as an 'effective' solvent embedding the model system show that specific activation or reaction energies can be modified by as much as 5 kcal mol^{-1}, but general trends are not changed.

Thus, in the absence of specific steric effects, the general trends issuing from our computations can be considered quite representative of the reaction mechanism governing the formation of tandem lesions.

4. Conclusions

Our study has enabled us to point out the different formation mechanisms of the TÂ and AT̂ tandem lesions. From one side, the computed thermodynamic parameters are in agreement with the available experimental data thus suggesting that the reaction mechanism issuing from our computations is reliable. From the other side, the discovery of a second reaction channel for the 5′-AT-3′ route could explain the excess of the AT̂ tandem lesions and the low proportion of TÂ tandem lesions. This hypothesis appears reasonable in view of the known structure of the corresponding methylated guanine and opens interesting perspectives for further experimental investigations.

References

1 J. F. Ward, *Int. J. Radiat. Biol.*, 1994, **66**, 427.
2 M.-H. David-Cordonnier, S. S. Boiteux and P. O'Neill, *Nucleic Acids Res.*, 2001, **29**, 1107.
3 J. G. Blaisdell and S. S. Wallace, *Proc. Natl. Acad. Sci. U. S. A.*, 2001, **98**, 7426.
4 H. C. Box, E. E. Budzinski, J. B. Dawidzik, J. S. Gobey and H. G. Freund, *Free Radical Biol. Med.*, 1997, **23**, 1021.
5 J. Cadet, M. Berger, T. Douki and J. L. Ravanat, *Rev. Physiol. Biochem. Pharmacol.*, 1997, **131**, 1.
6 J. Cadet and P. Vigny, *Bioorganic Photochemistry. Photochemistry and the Nucleic Acids, vol. 1*, Wiley and Sons, New York, 1990, pp. 1–272.
7 A. G. Bourdat, T. Douki, S. Frelon, D. Gasparutto and J. Cadet, *J. Am. Chem. Soc.*, 2000, **122**, 4549.
8 T. Douki, J. Rivière and J. Cadet, *Chem. Res. Toxicol.*, 2002, **15**, 445.
9 J. Cadet, T. Douki, D. Gasparutto and J.-L. Ravanat, *Mutat. Res.*, 2003, **531**, 5.
10 A.-G. Bourdat, D. Gasparutto and J. Cadet, *Nucleic Acids Res.*, 1999, **27**, 1015.
11 A. Gentil, F. Le Page, J. Cadet and A. Sarasin, *Mutat. Res.*, 2000, **452**, 51.
12 Z. Liu, Y. Gao and Y. Wang, *Nucleic Acids Res.*, 2003, **31**, 5413.
13 Z. Liu, Y. Gao Zeng, F. Fang, D. Chi and Y. Wang, *Photochem. Photobiol.*, 2004, **80**, 209.
14 M. Dizdaroglu, *Biochem. J.*, 1986, **238**, 247.
15 R. Flyunt, R. Bazzanini, C. Chatgilialoglu and Q. G. Mullazani, *J. Am. Chem. Soc.*, 2000, **122**, 4225.
16 I. Kuraoka, C. Bender, A. Romieu, J. Cadet, R. D. Wood and T. Lindahl, *Proc. Natl. Acad. Sci. U. S. A.*, 2000, **97**, 3832.
17 P. J. Brooks, D. S. Wise, D. A. Berry, J. V. Kosmoski, M. J. Smerdon, R. L. Somers, H. Mackie, A. Y. Spoonde, E. J. Ackerman, K. Coleman, R. E. Tarone and J. H. Robbins, *J. Biol. Chem.*, 2000, **255**, 22355.
18 I. Kuruoka, P. Robins, C. Masutani, F. Hanaoka, D. Gasparutto, J. Cadet, R. D. Wood and T. Lindahl, *J. Biol. Chem.*, 2000, **276**, 49283.
19 A. A. Shaw and J. Cadet, *Int. J. Radiat. Biol.*, 1988, **54**, 987.
20 A. Romieu, D. Gasparutto and J. Cadet, *J. Chem. Soc., Perkin Trans. 1*, 1999, **257**.
21 E. Muller, D. Gasparutto, M. Jaquinod, A. Romieu and J. Cadet, *Tetrahedron*, 2000, **56**, 8689.
22 J. R. Wagner, C. Decarroz, M. Berger and J. Cadet, *J. Am. Chem. Soc.*, 1999, **121**, 4101.
23 E. Muller, D. Gasparutto and J. Cadet, *ChemBioChem*, 2002, **3**, 534.
24 A. Romieu, S. Bellon, D. Gasparutto and J. Cadet, *Org. Lett.*, 2000, **2**, 1085.
25 S. Bellon, J.-L. Ravanat, D. Gasparutto and J. Cadet, *Chem. Res. Toxicol.*, 2002, **15**, 598.
26 H. Hong, H. Cao, Y. Wang and Y. Wang, *Chem. Res. Toxicol.*, 2006, **19**, 614.
27 C. Bienvenu, J. R. Wagner and J. Cadet, *J. Am. Chem. Soc.*, 1996, **118**, 11406.
28 Q. Zhang and Y. Wang, *J. Am. Chem. Soc.*, 2003, **125**, 12795.
29 Q. Zhang and Y. Wang, *Nucleic Acids Res.*, 2005, **33**, 1593.
30 W. Kock and W. C. Holthousen, in *A Chemist's Guide to Density Functional Theory*, Weinheim, Wiley-VCH, 2000.
31 C. Adamo, M. Cossi, N. Rega and V. Barone, in *Theoretical Biochemistry: Processes and Properties of Biological Systems. Theoretical and Computational Chemistry, vol. 9*, Elsevier, New York, 2001.
32 R. B. Zhang and L. A. Eriksson, *Chem. Phys. Lett.*, 2006, **417**, 303.
33 M. J. Frisch, G. W. Trucks, H. B. Schlegel, G. E. Scuseria, M. A. Robb, J. R. Cheeseman, J. A. Montgomery, Jr., T. Vreven, K. N. Kudin, J. C. Burant, J. M. Millam, S. S. Iyengar, J. Tomasi, V. Barone, B. Mennucci, M. Cossi, G. Scalmani, N. Rega, G. A. Petersson, H. Nakatsuji, M. Hada, M. Ehara, K. Toyota, R. Fukuda, J. Hasegawa, M. Ishida, T. Nakajima, Y. Honda, O. Kitao, H. Nakai, M. Klene, X. Li, J. E. Knox, H. P. Hratchian, J. B. Cross, V. Bakken, C. Adamo, J. Jaramillo, R. Gomperts, R. E. Stratmann, O. Yazyev, A. J. Austin, R. Cammi, C. Pomelli, J. Ochterski, P. Y. Ayala, K. Morokuma, G. A. Voth, P. Salvador, J. J. Dannenberg, V. G. Zakrzewski, S. Dapprich, A. D. Daniels, M. C. Strain, O. Farkas, D. K. Malick, A. D. Rabuck, K. Raghavachari, J. B. Foresman, J. V. Ortiz, Q. Cui, A. G. Baboul, S. Clifford, J. Cioslowski, B. B. Stefanov, G. Liu, A. Liashenko, P. Piskorz, I. Komaromi, R. L. Martin, D. J. Fox, T. Keith, M. A. Al-Laham, C. Y. Peng, A. Nanayakkara, M. Challacombe, P. M. W. Gill, B. G. Johnson, W. Chen, M. W. Wong, C. Gonzalez and J. A. Pople, *GAUSSIAN 03 (Revision C.02)*, Gaussian, Inc., Wallingford, CT, 2004.
34 A description of basis sets and standard computational methods can be found in *Exploring Chemistry with Electronic Structure Methods, 2nd edn*, ed. J. B. Foresman and A. E. Frisch, Gaussian Inc., Pittsburg, PA, 1996.
35 C. Gonzalez and H. B. Schlegel, *J. Phys. Chem.*, 1990, **16**, 1170.
36 B. Durbeej and A. L. Eriksson, *J. Photochem. Photobiol., A*, 2002, **152**, 95.
37 B. Durbeej and A. L. Eriksson, *Photochem. Photobiol.*, 2003, **78**, 159.
38 F. Jolibois, A. Grand, J. Cadet, C. Adamo and V. Barone, *Chem. Phys. Lett.*, 1999, **301**, 255.
39 R. Improta and V. Barone, *Chem. Rev.*, 2004, **104**, 1231.
40 M. Cossi, G. Scalmani, N. Rega and V. Barone, *J. Chem. Phys.*, 2002, **117**, 43.
41 M. F. Iozzi, M. Cossi, R. Improta, N. Rega and V. Barone, *J. Chem. Phys.*, 2006, **124**, 184103.

